Talanta 87 (2011) 126–135

Contents lists available at SciVerse ScienceDirect

Talanta

journal homepage: www.elsevier.com/locate/talanta

Novel CeO_2-based screen-printed potentiometric electrodes for pH monitoring

S. Betelu [a,*], K. Polychronopoulou [b], C. Rebholz [b], I. Ignatiadis [a]

[a] BRGM, Environment and Processes Division, 45060 Orléans Cedex 2, France
[b] Mechanical and Manufacturing Engineering Department, University of Cyprus, 1678 Nicosia, Cyprus

ARTICLE INFO

Article history:
Received 23 March 2011
Received in revised form
23 September 2011
Accepted 27 September 2011
Available online 1 October 2011

Keywords:
pH sensing
Cerium-based oxides
Mass modified screen-printed electrodes
Monitoring

ABSTRACT

Nuclear waste repositories are being installed in deep excavated rock formations in some places in Europe to isolate and store radioactive waste. In France, the Callovo-Oxfordian formation (COx) is a possible candidate for nuclear waste storage. This work investigates the applicability of CeO_2-based oxides (CeO_2, $Ce_{0.8}Sm_{0.2}O_2$ and $Ce_{0.8}Zr_{0.2}O_2$) for monitoring the pH of the COx pore water ($T = 25\,^{\circ}C$). The study is limited to the pH range between 5.5 and 13.2, which includes the pH values that have been encountered or are anticipated in the COx formation during its evolution as radioactive waste repository due mainly to alkalinisation, an increase in salinity, and a decrease in redox potential. Screen-printing was done to assemble electrodes and rapidly generate data sets. The electrochemical behavior of CeO_2-based screen-printed electrodes (CeO_2-based SPEs) was determined by cyclic voltammetry and electrochemical impedance spectroscopy. The use of the electrodes for pH sensing was then evaluated by potentiometric measurements. The feasibility of measuring pH with CeO_2-based SPEs was first tested in NH_4Cl/NH_3 buffer solutions, leading to electrode calibration over the widest range of pH, from around neutral to basic pH. Experiments were then conducted in $NaHCO_3/Na_2CO_3$ buffer samples similar to conditions prevailing in the COx formation. $Ce_{0.8}Zr_{0.2}O_2$ SPEs exhibit a near-Nernstian behavior (sensitivity $-(51 \pm 2)$ mV/pH) in the pH range of 5.5–13.2 at 25 °C. Electrode response was slightly affected by the direction of the pH change. Electrode reliability was clearly demonstrated for pH monitoring. Probes based on the same components, but more durably designed, could be considered for pH measurements in radioactive waste repositories.

1. Introduction

Radioactive waste repositories are being installed in deep excavated rock formations in some places in Europe to isolate and store radioactive waste. It is therefore necessary to measure, in situ, the health of the structure throughout its life. The near-field rock can be monitored and knowledge of any geochemical transformations can be acquired using sensors, thus enabling the sustainable management of long-term safety, reversibility and retrievability [1]. The most significant chemical parameters are pH, conductivity and redox potential.

pH is one of the most important parameters characterizing samples [2]. Extensive efforts have been devoted to developing highly sensitive analytical procedures for measuring pH. There is, however, an increasing need for sensing probes for continuous measurements on site and their development represents a serious challenge in terms of accuracy, repeatability and particularly robustness.

Based on reversible interfacial redox processes that involve protons [3,4], metal oxide potentiometric electrodes have been regarded as the most promising technologies for pH measurements [3–19] due to their intrinsic mechanical stability with regard to temperature, pressure and aggressive environments [3,20]. Furthermore, oxide-based electrodes have the advantage of being easily miniaturized [3,20,21].

Niedrach [22,23] was the first to report on the application of zirconium oxide (zirconia, ZrO_2) membrane-type potentiometric sensors for pH measurements. However, this membrane electrode exhibited only a near-Nernstian-pH response at high temperatures [24,25] and, because of their high impedance [26], pH sensors with zirconia membranes were reported to exhibit sluggish and subtheoretical responses at temperatures below 150 °C [27]. The study of new zirconia-based materials with higher ionic conductivity should extend the operating temperature limits.

Compared to zirconia, CeO_2 (ceria) has a considerably higher oxide-ion conductivity [28,29]. Moreover, because of its particular and unique properties, cerium, a rare earth element (REE), might be used for robust, long-term sensors. Indeed, cerium's Eh–pH diagram differs from those of other REEs [30]. Cerium has a Ce(IV) valence in addition to Ce(III) and large pe–pH domain for the Ce(IV) species. CeO_2 dominates much of the water stability field. This field also covers much of the Ce^{3+} field as well. Furthermore, it is a non-stoichiometric n-type semiconductor with oxygen vacancies as predominant ionic defects, and the oxygen-vacancy

* Corresponding author. Tel.: +33 238643268; fax: +33 238643062.
E-mail address: s.betelu@brgm.fr (S. Betelu).

0039-9140/$ – see front matter © 2011 Elsevier B.V. All rights reserved.
doi:10.1016/j.talanta.2011.09.051

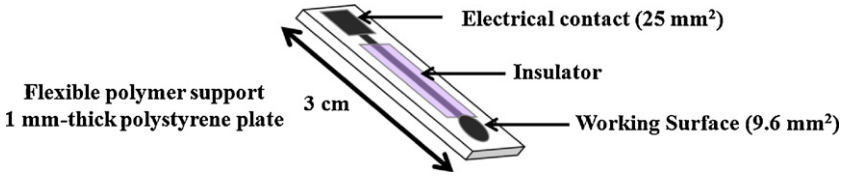

Fig. 1. Scheme of a screen-printed electrode.

concentration as well as oxide-ion conductivity in CeO_2 can be increased by substitution. Balazs and Glass showed that, of all the ceria solid electrolytes, $Ce_{0.8}Sm_{0.2}O_2$ had the highest oxide ion conductivity [28]. Samarium-substituted ceria ceramic membrane-type pH sensors have been reported to exhibit a Nernstian slope in buffer solutions at 75 °C [31,32]. It would, therefore, be of great interest to use binary compositions, especially Zr-substituted ceria oxides, to improve the sensitivity of sensors for pH monitoring at lower temperatures.

In the study reported here, the possible use of a CeO_2-based electrode (CeO_2-, $Ce_{0.8}Sm_{0.2}O_2$- and $Ce_{0.8}Zr_{0.2}O_2$-based screen-printed electrodes (SPEs)) was investigated for continuous pH measurements. An Sm-substituted ceria oxide composition was synthesized as described by Balazs and Glass [28] and was also studied for Zr-substituted ceria oxide. Moreover, these Ce-rich compositions preserved the cubic fluorite lattice of CeO_2, which has beneficiary properties such as high oxygen storage capacity (OSC) [33]. The screen-printing process was chosen as the most appropriate technology for assembling reproducible electrodes [34,35] and rapidly generating data sets. This technology has been used to develop electrodes based on PdO, TiO_2, PtO_2 [14], RuO_2 [14,36] and CoO_2 [37]. Of these, the RuO_2- and CoO_2-based electrodes were reported to be the most sensitive. Nevertheless, carbon-based mass-modified RuO_2 screen-printed electrodes only exhibited a near-Nernstian behavior $-(51.2 \pm 0.1)$ mV/pH in the non-alkaline pH range (2–7) [14]. In comparison, ruthenium dioxide–glass composite demonstrated a Nernstian behavior between pH 2 and 12 and therefore might be used as a pH sensor [36]. However, these electrodes only exhibited long-term mechanical stability between pH 5 and 9, probably due to mechanical strain owing to pH-dependent expansion and contraction of a hydrated phase within the composite. Concerning the CoO_2-based electrodes, the optimization of both the nature and the amount of the incorporated salt led to an electrode exhibiting a Nernstian behavior in the pH range of 2–12. Moreover, these electrodes worked for 5 days at pH 4 with a relative standard deviation of about 10%. However, their robustness for alkaline pH has not been verified.

In this study, CeO_2-based SPE performance levels, reliability and robustness for pH determination were investigated by potentiometric measurements at 25 °C. Only the pH range that includes previously encountered or anticipated pH values in the Callovo-Oxfordian formation (COx) during its evolution as a radioactive waste repository (pH 6–13) were studied. The feasibility of the pH electrodes was first tested in NH_4Cl/NH_3 buffer solutions, which led to electrode calibration over the widest range of pH, from around neutral to basic pH. Experiments were also conducted in $NaHCO_3/Na_2CO_3$ buffer samples similar to conditions prevailing in the COx formation [38].

2. Materials and methods

2.1. Synthesis of CeO_2-based powders

Cerium oxide (CeO_2, $Ce_{0.8}Sm_{0.2}O_2$ and $Ce_{0.8}Zr_{0.2}O_2$) powders were synthesized using procedures similar to those previously described [39].

2.2. Sensor assembly

2.2.1. Ink preparation

CeO_2-based inks were prepared by adding CeO_2-based powders (CeO_2 50% (w/w)) directly to a commercial carbon-based ink (Electrodag PF 407A from Acheson, a mixture of carbon black (particle size lower than 1 μm) and graphite carbon (particle size ranging from 8.5 μm (255×10^{-6} in.) to 18 μm (540×10^{-6} in.))). The mixture was stirred by hand for 5 min prior to the printing process.

2.2.2. Screen-printing

A manual screen-printer (from Circuit Imprimé Français, France) was used to make the sensors. An array of six electrodes was printed on 1 mm-thick polystyrene plates (Sericol) by forcing the conductive ink through the mesh of a polyester screen stencil (77 threads cm^{-1}, Circuit Imprimé Français, France).

After drying (1 h at room temperature) and curing (1 h in an oven at 60 °C), a layer of insulation (a thin layer of polystyrene dissolved in mesitylene (Fluka Analytical, France), which evaporates slowly, in 2 days, at room temperature) was spread by hand over the conductive track (20 mm × 1 mm), leaving a 9.6-mm^2 working disk area and a 25-mm^2 square tip for electrical contact (Fig. 1). In accordance with Cagnini et al. [40] and Koncki et al. [14], the typical thickness of the film was around 20 μm. The screen-printing process enabled the assembly of small batches of approximately 20 electrodes.

Unmodified carbon-based SPEs (C SPEs) were also prepared by screen-printing with the commercial ink without any modification in order to compare the properties of CeO_2-based SPEs to carbon electrodes (reference samples).

2.3. Measurements

2.3.1. Apparatus

All the potentials were measured with respect to the saturated calomel electrode (SCE), which consisted of a commercial SCE protected with a KCl 3 mol L^{-1} junction. The junction potential is less than 1 mV at 25 °C. The difference in voltage was measured with a millivolt-meter between protected and unprotected SCE, both immersed in NaCl 0.1 mol L^{-1}. All potential values herein are expressed in volts (V) with respect to the normal hydrogen electrode (NHE) scale by adding 245 mV.

DC electrochemical techniques were used on thermostated samples using a potentiostat-galvanostat (Princeton Applied Research, Tennessee, USA) PAR model-2273, interfaced to a PC system with PAR's PowerSuite v.2.58 software. A platinum wire was used as an auxiliary electrode. The working solution volume was 10 mL.

Cyclic voltammetry (CV) measurements were done at 50 mV s^{-1} between −0.8 V/NHE and 1.7 V/NHE. Electrochemical impedance spectroscopy (EIS) measurements were done over a frequency range of 10 μHz to 1 MHz using perturbation signals with an amplitude of 5 mV. The computer-assisted evaluation of the impedance spectra was done with the PAR-2273 impedance measurement system using an integrated data-acquisition and analysis system and the ZSimpWin version 3.21 software (Echem Software, Bruno Yeum, Ann Arbor, MI, USA).

Table 1
Preparation of 1 L of NH_4Cl/NH_3 and $NaHCO_3/Na_2CO_3$ buffer solutions.

NH_4Cl/NH_3 buffer solutions					
	pH	Volume (mL) of		Total equivalent activity of	
		HCl (1 mol L^{-1})	NH_3 (1 mol L^{-1})	NH_4^+ (mol L^{-1})	NH_3 (mol L^{-1})
	7.2	50.0	50.7	3.4×10^{-2}	3.0×10^{-4}
	7.5	50.0	51.1	3.4×10^{-2}	6.3×10^{-4}
	7.6	50.0	50.3	3.4×10^{-2}	8.0×10^{-4}
	8.6	50.0	60.0	3.4×10^{-2}	8.0×10^{-3}
	9.3	50.0	97.0	3.3×10^{-2}	3.8×10^{-2}
	9.5	50.0	125.0	3.3×10^{-2}	5.9×10^{-2}
	9.7	50.0	170.0	3.2×10^{-2}	9.2×10^{-2}
	10.6	50.0	950.0	2.2×10^{-2}	4.5×10^{-1}
	10.8	30.0	970.0	1.4×10^{-2}	4.7×10^{-1}
$NaHCO_3/Na_2CO_3$ buffer solutions					
IS[a]	pH	Volume (mL) of		Total equivalent activity of	
		$NaHCO_3$ (1 mol L^{-1})	Na_2CO_3 (1 mol L^{-1})	HCO_3^- (mol L^{-1})	CO_3^{2-} (mol L^{-1})
0.05	8.6	53.0	22.0	3.8×10^{-2}	1.2×10^{-3}
	8.9	43.0	3.6	3.1×10^{-2}	1.8×10^{-3}
	9.7	21.8	9.4	1.6×10^{-2}	4.7×10^{-3}
0.10	9.6	45.3	18.2	3.1×10^{-2}	8.3×10^{-3}
	10.1	24.9	22.3	1.8×10^{-2}	1.0×10^{-2}
	10.6	7.1	30.8	5.3×10^{-3}	1.4×10^{-2}
0.20	9.3	115.7	28.2		
	10.1	36.1	54.6		
	10.4	19.3	60.1		
	10.6	12.3	62.4		
	11.8	3.9	64.9		

[a] Ionic strength.

Potentiometric measurements were recorded continuously in thermostated samples with a digital multimeter and data acquisition system (Keithley instruments, model 2700, Cleveland, OH, USA). The sample volume was 100 mL. CeO_2-based SPEs pH-sensing characteristics were evaluated by measuring their open-circuit potential (OCP) versus SCE. The pH values of all samples and buffer solutions were monitored with a commercial glass electrode that was calibrated daily using commercial standard buffer solutions.

2.3.2. Solutions

All experiments were done at a constant temperature ($T = 25.00 \pm 0.04\,^{\circ}C$) under continuous stirring (about 200 rpm) in NaCl 0.1 mol L^{-1}, NH_4Cl/NH_3 or $NaHCO_3/Na_2CO_3$ buffer solutions. The preparation of 1 L of the buffer solutions is summarized in Table 1. PHREEQC® geochemical code was used to determine the total equivalent activity of the different ions with the appropriate associated thermodynamic database (THERMODEM® thermodynamic database generated by BRGM). It is worth noting that no Pitzer database was available at BRGM. The thermodynamic calculations were not investigated for supporting electrolyte which ionic strength was higher than 0.1 mol L^{-1}.

3. Results and discussion

3.1. SPE assembly and electrochemical characterization

3.1.1. Electrode assembly

The screen-printing process was selected as the most appropriate technology for making reproducible electrodes [34,35] and rapidly generating data sets. It involves transferring a thin layer of a conductive ink onto a rigid substrate through the mesh of a screen pattern [41]. Polyester screens are usually used for printing, with patterns designed in accordance with the analytical purpose in mind [42]. The ink is made up of (i) the active material, which ensures conductivity: a powder of conductive particles (maximal particle size: 10 μm), (ii) a binder, which ensures cohesion by linking the active material and the substrate, and (iii) an organic solvent, which gives the right rheological properties. The solvent is removed by drying and/or heating. The composition of the ink determines the selectivity as well as the sensitivity of the sensor. The direct addition of CeO_2-based oxides to the commercial carbon-based ink prior to the printing process was tested in order to simplify electrode assembly. Various proportions of CeO_2-based powders (up to 80% (w/w)) were added to the conductive ink, the aim being to add as much as possible. The carbon-based ink ensured both conductivity and cohesion. 50% (w/w) was found to be the highest amount of CeO_2 possible to produce (i) ink fluid enough to be spread as a single layer (thickness ≅ 20 μm [14,40]) on the stencil and (ii) a matrix that ensured consistency and enabled the adhesion of electrodes to the flexible support.

The influence of the composition of the CeO_2-based ink on the electrochemical characteristics (i.e. potential range, capacitive current, conductive properties and electrode/solution interface characterization) of each type of CeO_2-based SPE was determined by CV or EIS measurements. The results were compared to those obtained with unmodified C SPEs. All experiments were done in 10 mL of NaCl 0.1 mol L^{-1} solution. For each type of SPE, tests were done with five different electrodes.

3.1.2. Potential range

The potential range, which is the window of potential values in which the reduction or oxidation of species can be observed, determines the electrode polarization domain [43]. The reduction of protons (towards H_2) determines the polarization domain towards the negative potentials, whereas oxidation of (i) the water (towards O_2) or (ii) the electrode material constitutes the positive limit.

SPE potential ranges were determined from the voltammograms obtained by CV (Fig. 2).

CeO_2-based SPEs have a potential window as wide as those of unmodified carbon-based SPEs, ranging from −0.1 V/NHE to

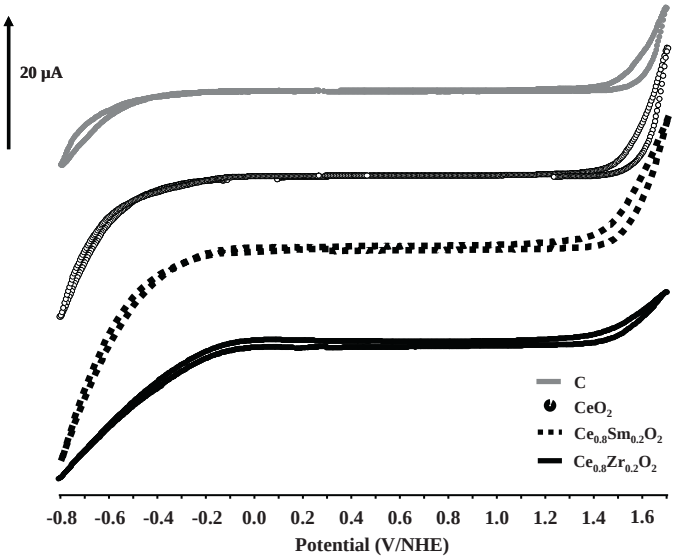

Fig. 2. C-, CeO_2-, $Ce_{0.8}Sm_{0.2}O_2$- and $Ce_{0.8}Zr_{0.2}O_2$-based SPEs cyclic voltammograms recorded in NaCl 0.1 mol L^{-1}. Experimental conditions: CV between −0.8 V/NHE and +1.7 V/NHE. Scan rate: 0.05 V s^{-1}, 5 electrodes.

+1.4 V/NHE. This shows that these electrodes behave as almost inert materials working over a wide potential range at a given pH.

3.1.3. Capacitive current

Capacitive current values were obtained for $E = 0.7$ V/NHE from the voltammograms recorded by CV (Table 2). In agreement with the literature, C SPEs have a very low capacitive current [42,44]. A similar result was obtained for CeO_2 SPEs, due to the high exchange current density of CeO_2 [28].

Cerium substitution by samarium or zirconium led to an increase in the charging current by factors of 6.5 and 12.0 for $Ce_{0.8}Sm_{0.2}O_2$ SPEs and $Ce_{0.8}Zr_{0.2}O_2$ SPEs, respectively. This might be due to the fact that oxygen vacancies are the main charge carriers for $Ce_{0.8}Sm_{0.2}O_2$ SPEs and $Ce_{0.8}Zr_{0.2}O_2$ SPEs. The difference between $Ce_{0.8}Sm_{0.2}O_2$ and $Ce_{0.8}Zr_{0.2}O_2$ can be assigned to the difference in microstructure. This can be expressed in terms of the different extent of distortion due to expected different solid solubility, as implied by the different ionic radii of Sm^{3+} (1.04 Å), Ce^{4+} (1.01 Å) and Zr^{4+} (0.72 Å). However, the capacitive current observed was of the same order of magnitude as that of the solid electrodes [44], which meant that high-input impedance equipment was not needed for subsequent measurements. These results suggest a greater sensitivity of the newly assembled SPEs compared to those described in the literature [23–25,27,45], which work at temperatures below 150 °C.

3.1.4. Conductive properties

The study of the conductive properties of each type of SPE involved comparing the cyclic voltammograms obtained with the SPEs and the electrochemical behavior of Fe(III)/Fe(II) using the ferrocenylmethyl-trimethyl-ammonium hexafluorophosphate probe [46].

Table 2
SPEs capacitive current obtained in NaCl 0.1 mol L^{-1}. Experimental conditions: CV between 0.1 V/NHE and 1 V/NHE. Scan rate: 0.05 V s^{-1}, 5 electrodes.

SPEs	I_c (nA)
C	36 ± 1
CeO_2	40 ± 2
$Ce_{0.8}Sm_{0.2}O_2$	260 ± 10
$Ce_{0.8}Zr_{0.2}O_2$	470 ± 20

Table 3
$|\Delta E|$ (mV) as well as anodic and cathodic i_p (nA) measured by CV in NaCl 0.1 mol L^{-1} containing $FcTMA^+$ 2×10^{-3} mol L^{-1}. Experimental conditions: CV between 0.1 V/NHE and 1 V/NHE. Scan rate: 0.05 V s^{-1}, 5 electrodes.

SPEs	$\|\Delta E\|$ (mV)	i_{pa} (nA)	i_{pc} (nA)
C	62 ± 2	195 ± 10	195 ± 10
CeO_2	63 ± 3	205 ± 10	205 ± 10
$Ce_{0.8}Sm_{0.2}O_2$	60 ± 3	205 ± 10	205 ± 10
$Ce_{0.8}Zr_{0.2}O_2$	60 ± 3	205 ± 10	205 ± 10

The difference $|\Delta E|$ (Table 3) between the oxidation and reduction peaks of the Fe(III)/Fe(II) couple made it possible to estimate the speed of electronic charge transfer of the CeO_2-based SPE compared to that of unmodified SPEs. The intensity of the anodic and catholic peaks (i_p) made it possible to estimate the reversibility at the electrode of the well-known reversible redox phenomenon.

The cathodic and anodic peak currents are the same and reproducible (relative standard deviation, RSD < 5%) for all types of SPEs, which shows the reversibility of the redox phenomenon at the working surfaces. Measured $|\Delta E|$ values were close to the theoretical values for rapid electron transfer (56 mV) [43], which shows that no decrease in the electron transfer rate is observed when electrodes were modified by CeO_2-based oxides.

3.1.5. Electrochemical impedance measurements and their interpretation

Impedance measurements were performed to investigate the elementary phenomena encountered at the electrolyte/electrode interfaces of CeO_2-based SPEs. They were compared to those obtained with C SPEs.

The EIS diagrams obtained (also shown in the Bode mode in Fig. 3C) were analyzed using the ZSimpWin software (version 3.21 by Bruno Yeum, Ann Arbor, MI, USA). Data processing makes it possible to read the data in terms of an equivalent electric circuit (EEC) obtained with a very close fit. The interpretation of impedance measurements and simulation then led to the determination of an EEC model, representing the behavior of the electrode/solution interface. This involves extracting the parameters from a model starting with impedance data, or in other words, seeking a model for which the impedance matches the measured data.

After modeling, using the EIS data obtained on the four disk-shaped oxide SPEs, two possible EECs are established (Fig. 4). It appears that all of the EIS diagrams can be described by these two EEC for all electrodes (Fig. 4). Both diagrams are the same (each EEC model was well fitted to data). Almost all of the parameters were obtained with an error lower than 5%. On the other hand, this implies that only the values of the parameters of the obtained EEC will change when the nature of the electrode changes.

For the different electrodes, the variations under the same experimental conditions result in different parameter values for each component of the exposed EEC (Table 4). The chi-square test (χ^2 test) was done for each simulation and enabled us to confirm that the results given by the model matched the measured values (reduced values). The electrode surface is about 10 mm^2 (or 0.1 cm^2).

R represents dc-resistance (in admittance $1/R$), C represents capacitor (in admittance $i\omega C$) and Q is a constant phase element (CPE) or equivalent capacitance and corresponds to a semi-infinite diffusion or an imperfect (leaking) capacitor. Q (in admittance is $Y_o(i\omega)^n$) is characterized by two parameters, Y_o, which is the Warburg (W) element parameter, and n. When $n = 1$, Q is only a C (capacitor).

The form of the impedance, in Nyquist mode, is an impedance of an immobile plane electrode immersed in an agitated electrolyte. It is an impedance of semi-infinite diffusion of type Q corresponding to a redox reaction (probably involving O_2). This type of impedance

Table 4
Results of the simulation of EIS measurements.

SPEs	EE circuit	Component of the equivalent electrical circuit (EEC)					
		R_e (ohm)	C_d (μF cm^{-2})	R_t (ohm)	Q–Y_o ($\times 10^6$)	Q–n	χ^2
CeO_2	R(C(RQ))	0.0	1.89	1587.0	0.556	0.927	0.0188
CeO_2	R(CR)Q	0.0	1.89	1583.0	0.556	0.927	0.0187
$Ce_{0.8}Sm_{0.2}O_2$	R(C(RQ))	0.0	0.63	5395.0	6.397	0.923	0.0073
$Ce_{0.8}Sm_{0.2}O_2$	R(CR)Q	0.0	0.63	5395.0	6.397	0.923	0.0073
$Ce_{0.8}Zr_{0.2}O_2$	R(C(RQ))	0.0	0.31	19,140.0	3.169	0.944	0.0088
$Ce_{0.8}Zr_{0.2}O_2$	R(CR)Q	0.0	0.31	19,140.0	3.169	0.944	0.0088
C	R(C(RQ))	0.0	1.20	2316.0	0.487	0.920	0.0101
C	R(CR)Q	0.0	1.20	2313.0	0.488	0.920	0.0101

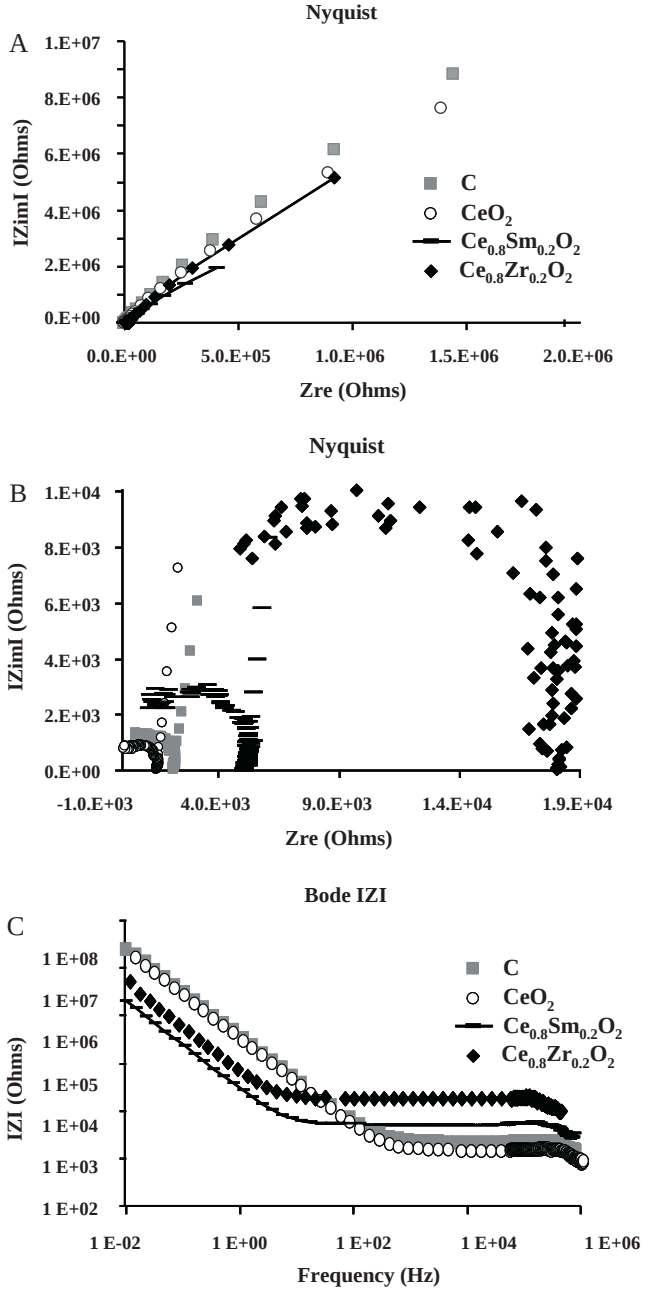

Fig. 3. (A) EIS diagrams in Nyquist mode. (B) EIS diagrams in Nyquist mode with magnification. (C) EIS diagrams in Bode mode, obtained with C- and CeO_2-based SPEs in aerated NaCl 0.1 mol L^{-1}. Experimental conditions: frequency range 10 Hz–1 MHz at +0.7 V/NHE, 5 electrodes.

intervenes in the reactions of the electrode when there is material transport by diffusion in a semi-infinite (in volume) phase.

Except for R_e, which is the electrolyte resistance (in ohms) and is very low (because of the high conductivity of the NaCl 0.1 mol L^{-1} supporting electrolyte), the EIS diagram shows that at least two distinct phenomena occur simultaneously at the electrode/solution interface during measurement.

The limiting process – the one that has the slowest kinetics – corresponds to the low frequencies and is shown by an almost straight line. It seems to be invariable with time and corresponds to the mass transport (diffusion-convection) at the electrode/solution interface (either to the dissolved oxygen required for oxidizing the substrate or to another redox phenomenon). The component Q gives a depressed semicircle and represents the flow variation of ions or molecules and the pure diffusion of these species. As n is near to 1, Q is almost a capacitor.

For the high-frequency (on the left), the loop obtained for all the electrodes is attributed to an elementary process by calculating the order of magnitude of its corresponding capacity C, defined by:

$$C_d = \frac{1}{2\pi\omega_0 R_t}$$

In this equation, C_d is the capacity in μF cm^{-2}, ω_0 is the maximum frequency in Hz, and R_t is the corresponding charge transfer resistance in ohms. The order of magnitude of the capacities obtained for all the electrodes is between 0.3 nF cm^{-2} ($Ce_{0.8}Zr_{0.2}O_2$ SPEs) and 1.9 nF cm^{-2} (CeO_2 SPEs), indicating very rapid phenomena. These values correspond to the capacities obtained during charge transfer, and the loop is a charge transfer loop. The values of R_t with each electrode show that R_t increases enormously when Sm and Zr are added to the CeO_2-based oxide, which shows that oxygen vacant sites are the charge carriers regulating these phenomena. $Ce_{0.8}Zr_{0.2}O_2$ oxide has the lowest C_d (0.3 nF cm^2) and the highest R_t (19,140 ohm), whereas CeO_2 oxide has the highest C (1.9 nF cm^2) and the lowest R_t (1585 ohm). These values are similar to those obtained by CV capacitive currents for theses oxides. Capacitive current for CeO_2 is low (40 μA), whereas it is very high for $Ce_{0.8}Zr_{0.2}O_2$ (470 μA), which could be attributed to the increased number of oxygen vacancies in the case of the latter.

The system identified by the impedances is relatively simple and involves mainly a charge transfer reaction. The transfer resistances obtained for the oxide SPEs are in very good agreement with

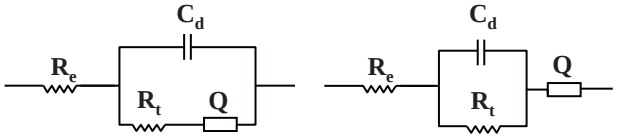

Fig. 4. Two indiscernible electrical equivalent circuits obtained from EIS diagram conducted with C- and CeO_2-based SPEs in NaCl (0.1 mol L^{-1}). Experimental conditions: frequency range 10 Hz–1 MHz at + 0.7 V/NHE, 5 electrodes.

the conductivities through the crystalline grains and the previously obtained results (see Section 3.1.3). As opposed to the results of Inda et al. [27], no grain boundary impedance was observed, probably due to the thinness of the SPEs. This suggests that $Ce_{0.8}Zr_{0.2}O_2$ SPEs are of interest for pH sensing at 25 °C.

The results demonstrate the possible use of CeO_2-based SPEs as electrochemical sensors and suggest higher sensitivity than with the ceria-, samaria- or zirconia-based electrodes described in the literature [23–25,27,45]. Their properties were therefore investigated for pH potentiometric measurements.

3.2. Analytical performance and robustness of CeO_2-based SPE pH sensors

The performance, reliability and robustness of CeO_2-based SPEs for pH determination were studied using potentiometric measurements at 25 °C (the ambient temperature in the COx formation). Only pH values similar to those that are anticipated in the COx formation when used as a radioactive waste repository were studied. Investigations were first done in NH_4Cl/NH_3 buffer solutions, after which the electrodes were calibrated for the widest pH range, from around neutral to basic pH. A carbonate/hydrogenocarbonate buffer system was then used since carbonate system equilibria constrain the pH of the clay rock's pore-water [38].

3.2.1. Feasibility study

The feasibility of measuring pH with CeO_2-based SPEs was first tested in NH_4Cl/NH_3 buffer solutions for a pH ranging from 7.2 to 10.8 (Fig. 5). The results were compared to those of C SPEs in order to determine whether the Ce-based oxides were of interest. Measurements for increasing and decreasing pH values were taken for 5 min, at a rate of one reading every 10 s.

The general convergence of the stabilization potential of all immersed SPEs revealed the occurrence of an equilibrium state under the experimental conditions. The CeO_2-based electrodes rapidly responded to changes in pH ($\leq$30 s) with regard to the relative standard deviation based on repeatability (RSD $\leq$ 3%). Furthermore, the equilibrium state remains unchanged with regard to pH variations, considering the relative standard deviation based on reproducibility (RSD $\leq$ 10%).

The voltage response of the electrodes to changing pH of the solution is linear. In aqueous solutions, the potential of CeO_2-based SPEs is governed by pH, presumably related to the ion-exchange properties of cerium oxide. When CeO_2-based SPEs come into contact with the solution, surface hydrolysis may occur and a proton exchange process creates an interfacial potential between the solution and the electrode surface. The difference in measured potential depends on pH when (i) the solution/oxide interface is reversible with respect to proton exchange and (ii) the oxide/substrate interface is electronically reversible. A single-phase oxygen intercalation in CeO_2-based oxides may be envisaged similar to the semiconducting oxide pH sensing mechanism proposed by Fog and Buck [3]. If we omit the water of hydration, we can assume that the electrode reaction is:

$$Ce(Sm/Zr)O_2 + 2nH^+ + 2ne^- \leftrightarrow Ce(Sm/Zr)O_{2-n} + nH_2O$$

A plot of the measured open-circuit potential versus the pH should yield a straight line with a Nernstian slope (e.g. −59.16 mV/pH at 25 °C) when the activity of oxygen in the substituted cerium oxide is assumed to be a constant. The slopes of the potential–pH curves of the three kinds of CeO_2-based SPEs and the C SPEs were studied. No Nernstian behavior was observed for C SPEs in the 7.5–11 range. A near-Nernstian behavior was observed for CeO_2-based SPEs, demonstrating the feasibility of potentiometric measurements with these kinds of working electrodes for pH determination

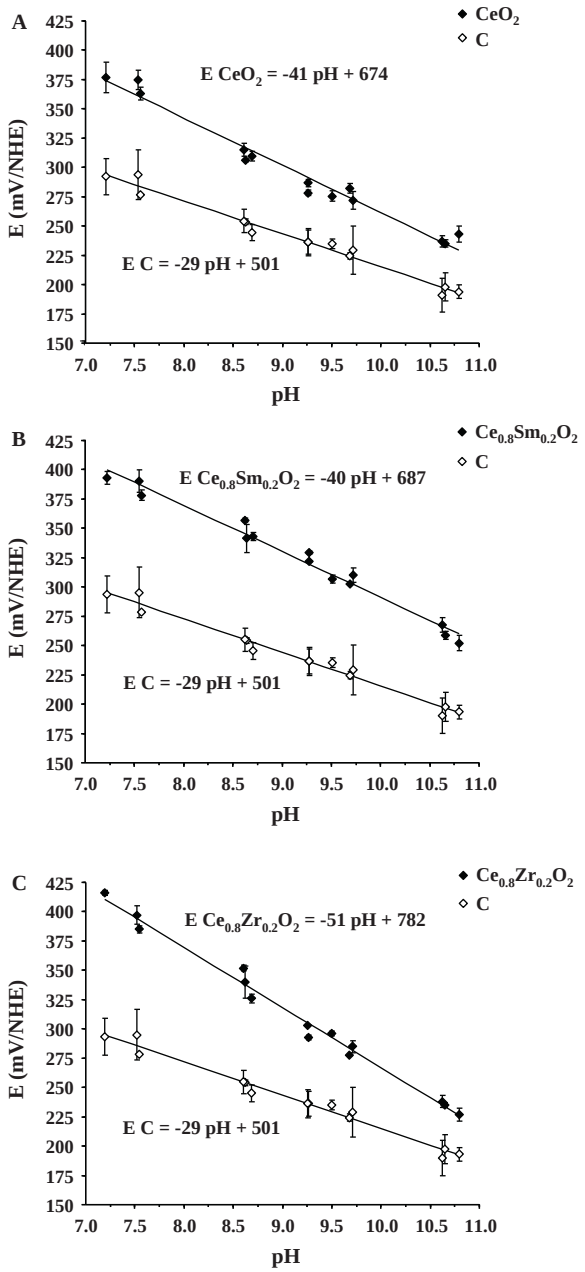

Fig. 5. Comparison between C- and (A) CeO_2-, (B) $Ce_{0.8}Sm_{0.2}O_2$- and (C) $Ce_{0.8}Zr_{0.2}O_2$-based SPEs potential (mV/NHE) versus pH in NH_4Cl/NH_3 buffer solutions at 25 °C.

in water samples. In accordance with [47–49] who established that proton conductive behavior depends on the oxygen vacancy concentration, the highest sensitivity for $Ce_{0.8}Zr_{0.2}O_2$ SPEs can be explained by $Ce_{0.8}Zr_{0.2}O_2$ being the highest oxygen vacancies carrier (see Section 3.1.4).

Zirconia membranes have been reported to be ideally suited to pH measurements at temperatures higher than 150 °C [24,25]. Sm-substituted ceria ceramic membrane-type pH sensors have been shown to have a Nernstian slope in buffer solutions at 75 °C [31,32]. It is worth noting that the previously mentioned studies [31,32] did not mention any unmodified ceria ceramic membrane to demonstrate that Sm was of interest. For the first time, in this work, CeO_2 SPEs, $Ce_{0.8}Sm_{0.2}O_2$ SPEs and $Ce_{0.8}Zr_{0.2}O_2$ SPEs were shown to have a nearly Nernstian behavior at 25 °C. All of these studies suggest that CeO_2-based electrodes are of interest for monitoring pH over the widest temperature range.

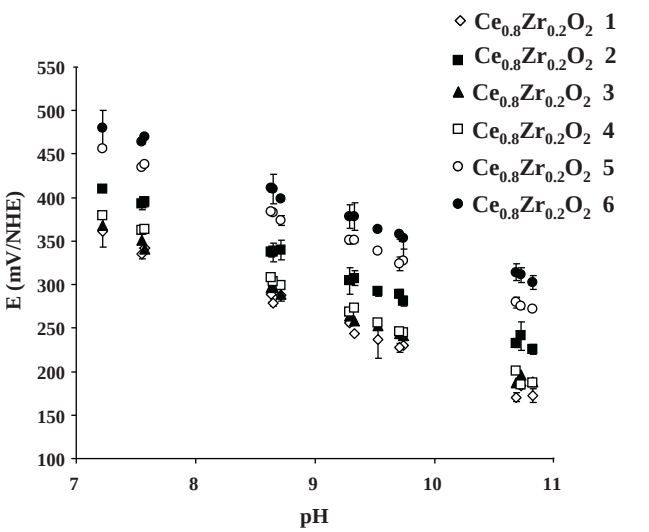

Fig. 6. Typical calibration curves obtained in NH_4Cl/NH_3 buffer solutions with $Ce_{0.8}Zr_{0.2}O_2$-based SPEs at 25 °C ($n = 6$ electrodes).

3.2.2. Repeatability and reproducibility

Repeatability was verified by carrying out repeated analyses with the same sensor in NH_4Cl/NH_3 buffer solutions (pH 7.6 and 8.6). Measurements were done for two hours at a rate of one reading per minute. RSD was ≤ 5% after 120 analyses, indicating that each type of SPE is reusable.

Reproducibility using different CeO_2-based SPEs was determined by producing a series of pH calibration curves with 12 electrodes from two different plates on each of which six electrodes were printed. Calibration curves were based on 25 replicates (one reading per minute) in the pH scale ranging from 7.2 to 10.8. Average sensitivity was $-(38 \pm 4)$ mV/pH, $-(40 \pm 4)$ mV/pH, $-(51 \pm 2)$ mV/pH for CeO_2-, $Ce_{0.8}Sm_{0.2}O_2$- and $Ce_{0.8}Zr_{0.2}O_2$-based SPEs, respectively. This is similar to the performance levels obtained for commonly used SPEs [34,35,44] and shows the convenience of CeO_2-based SPEs. Nevertheless, it is assumed that the measured potential results from a mixed potential carbon/CeO_2-based oxide. Typical measurements done with $Ce_{0.8}Zr_{0.2}O_2$-based SPE pH sensors (shown, for example, in Fig. 6: E° $Ce_{0.8}Zr_{0.2}O_2$-based SPEs = (780 ± 40)mV) show the need for electrode calibration before any measurements are done on natural samples, like for all other sensors described in the literature. Work is now being done to develop reproducible pH screen-printed electrodes that can be used without preliminary calibration. CeO_2-based oxide coated SPEs made by sputtering is foreseen.

3.2.3. Storage stability

The storage stability was studied by comparing the SPE analytical slopes in NH_4Cl/NH_3 buffer solutions of freshly printed electrodes with those obtained with electrodes from the same batch that had been stored 10 months at 25 °C (i) in the ambient air and (ii) in a N_2 inert glove-box. The conditions described above were used to compare the influence of carbon oxidation by atmospheric $O_2(g)$ and $H_2O(g)$.

Except for the unmodified carbon electrodes that were stored in the ambient air, for which the RSD on each measurement increased (from 5% ≤ RSD to RSD ≤ 15%), probably due to irreproducible carbon oxidation that led to the appearance of pH-sensing OH/COOH groups on the working surface, no significant difference in the pH potential slope was observed after the electrodes had been stored for 10 months. This (i) increases both the interest of and the stability of CeO_2-based oxides and (ii) suggests that the electrodes stored in a vacuum (to minimize carbon oxidation that would increase carbon hydrophilic properties [50–52]) were well suited to being integrated in an automated on-line analysis system for continuous monitoring without the need for maintenance over long periods.

3.2.4. Hysteresis effect

Solid oxide electrodes are subject to non-ideal effects such as hysteresis or memory effects that decrease the electrode accuracy and/or sustainability [3,53,54]. According to Bousse et al. [53], hysteresis or memory effects can be regarded as a delay of the voltage response versus pH.

Successive measurements were therefore taken using various devices for increasing and decreasing pH values in NH_4Cl/NH_3 buffer solutions to study the hysteresis effect of the sensing devices. Experiments carried out two times with the same electrode in both directions, from pH 7.2 to 10.8, indicated that there was no hysteresis with regards to the sensitivity of CeO_2-based SPEs (RSD ≤ 0.8%, $n = 4$ slopes for each electrode), showing that this kind of sensors is of interest for continuous measurements.

3.2.5. Influence of carbonate/hydrogenocarbonate buffer system and ionic strength

The potential developed by oxide-based electrodes is mainly the result of the hydrogen ion but can be modified by the presence of some complexing ions and/or their concentrations [55]. The influence of the carbonate/hydrogenocarbonate buffer system on the analytical response of the CeO_2-based SPEs was studied because carbonate system equilibria constrain the pH of the clay rock's pore-water [38]. Ionic strength was also investigated. Potentiometric measurements were done in $NaHCO_3/Na_2CO_3$, at ionic strengths ranging from 0.05 to 0.2 mol L^{-1} (Fig. 7). The experiment consisted in taking one reading every 30 s in each sample for 30 min.

The voltage response of SPEs versus pH remains linear in spite of the presence of carbonate and hydrogenocarbonate ions. Sensitivities were similar to those obtained in NH_4Cl/NH_3 buffer samples.

As regards the RSD based on reproducibility, neither ionic strength (in the range 0.05–0.2 mol L^{-1}) nor HCO_3^-/CO_3^{2-} ions present in natural waters affects the sensitivity of CeO_2-based SPEs, which suggests that they are of interest for pH measurements of the pore-water of the COx.

3.2.6. Calibration curves under atmospheric and anoxic conditions

In addition to measurements done under atmospheric oxygen saturation (with P_{O_2} about 0.2 atm) while the influence of the O_2/H_2O redox couple was being studied, several measurements were also done in a glove box (GB) in an oxygen-free atmosphere (100% nitrogen) at 25 °C.

These were done with reference to the anticipated decrease in the redox potential in the COx pore water caused by the decrease in the O_2 concentration. Fig. 8 shows the two calibration curves of the potential of the $Ce_{0.8}Zr_{0.2}O_2$-based SPEs versus pH under atmospheric (atm) and anoxic (GB) conditions. Data include measurements taken in NH_4Cl/NH_3 and $NaHCO_3/Na_2CO_3$ buffer solutions. The same measurements were also done using a 10-mm disk platinum electrode with a surface of 78.54 mm^2 (data not shown).

The potential of the platinum electrode (E_{Pt}) under atmospheric oxygen saturation is fixed by the O_2/H_2O redox couple. Under these conditions, E_{Pt} is governed by the PtO/Pt couple via $PtO + 2H^+ + 2e^- \Leftrightarrow Pt + H_2O$ with $E_{PtO/Pt}$ (mV) = 60.5 pH + 902, in agreement with Hoare [56] and Schüring et al. [57].

At the same pH and under aerobic conditions, a difference of about 120 mV (pH 0) is observed between Pt and $Ce_{0.8}Zr_{0.2}O_2$-based SPEs. This is of the same order of magnitude (about 180 mV) as for anoxic conditions where O_2/H_2O is the predominant redox couple with a very low quantity of oxygen. Moreover, the slope of the

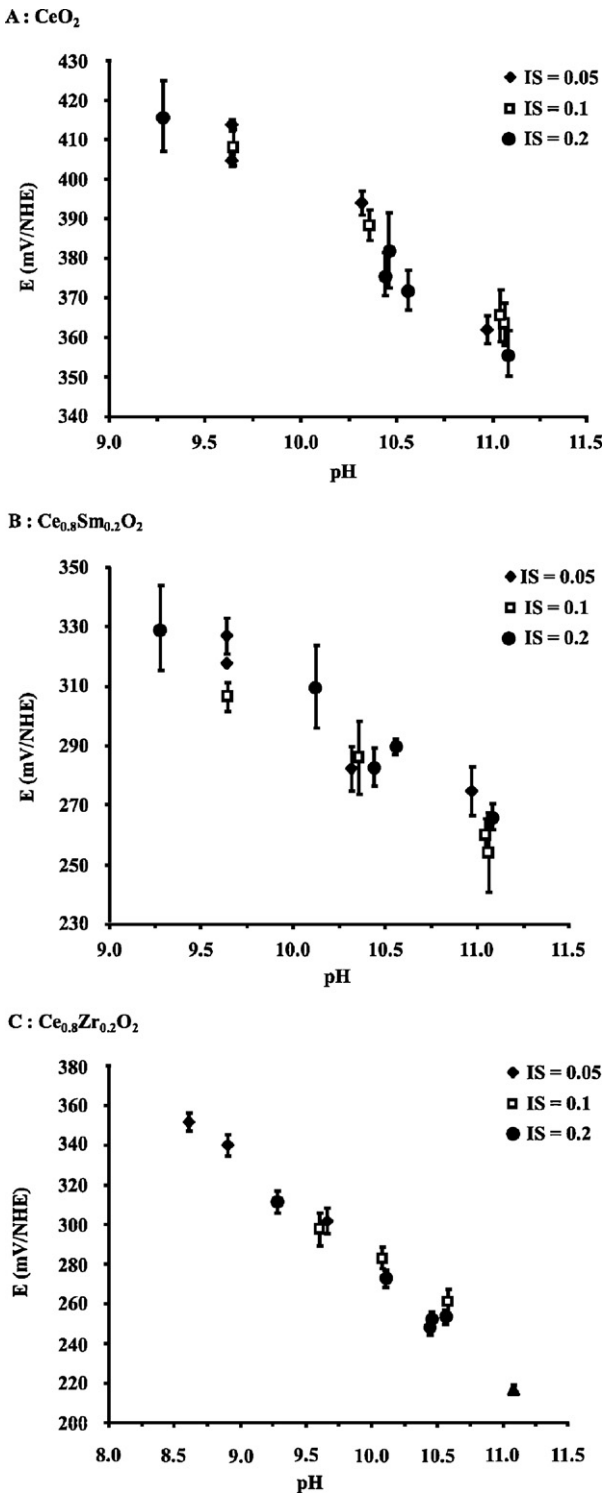

Fig. 7. Evolution of CeO_2-based SPEs potential (mV/NHE) according to pH as well as ionic strength. $NaHCO_3/Na_2CO_3$ buffer solutions.

potential–pH $Ce_{0.8}Zr_{0.2}O_2$-based SPEs remains the same regardless of the medium (51 mV), which is very important, while the intercept giving the potential at pH = 0 differs by about 110 ± 6 mV.

This shows the dependence, although weak, of the $Ce_{0.8}Zr_{0.2}O_2$-based SPE on the O_2/H_2O redox couple in the solution. This test provides information concerning the simultaneous but different behavior of two different electrodes under identical conditions and the same reference electrode. Knowledge of their electrochemical

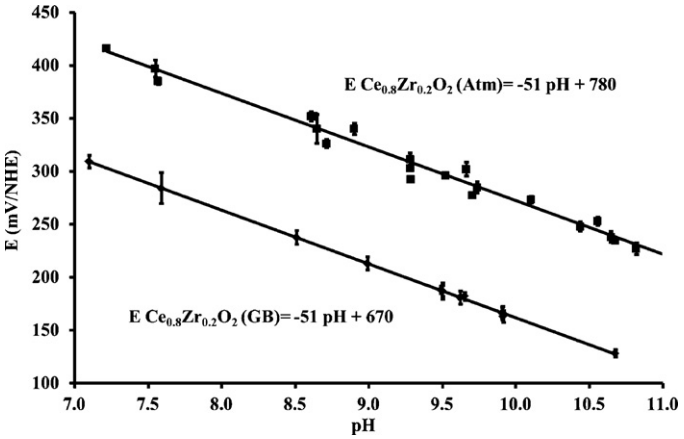

Fig. 8. $Ce_{0.8}Zr_{0.2}O_2$-based SPEs calibration curve obtained at 25 °C under atmospheric oxygen saturation (atm) and anoxic conditions carried out in a glove box (GB). Data include measurements conducted in NH_4Cl/NH_3 and $NaHCO_3/Na_2CO_3$ buffer solutions.

curves will allow us to draw potential–pH diagrams when observing and monitoring pH in the underground components of radioactive waste repositories where reference electrodes will not be used.

3.2.7. pH measurement applications: simulation of alkaline perturbation in the clay-rock pore-water

Large quantities of cement and concrete will be used in the geological storage facilities for long-lived radioactive waste. An alkaline plume ($9 \leq pH \leq 11$) diffusing from old concrete through the pore-water of argillite-type rocks was simulated. The pH in NaCl (0.1 mol L^{-1}, pH ≈ 5.5) spiked with a $NaHCO_3/Na_2CO_3$ buffer (pH 10.5, ionic strength 0.2) ($5.5 \leq pH \leq 10.2$) was continuously monitored using CeO_2-based SPEs and classical glass membranes (Fig. 9). Experiments were done twice between pH ≈ 5.5 and ≈8.6. The pH was then increased to 10.2. The samples containing $Ce_{0.8}Zr_{0.2}O_2$-based SPEs were then spiked with NaOH (1 mol L^{-1}) in order to evaluate the electrode performance up to $pH \geq 12$. One reading was recorded every 60 s for 36 h.

The first experiments (between pH ≈ 5.5 and ≈8.6) showed that the potential of the electrodes was somewhat affected by hysteresis. For a given potential E (mV/NHE), an uncertainty of 0.25 and 0.3 pH units was observed for CeO_2 as well as for $Ce_{0.8}Zr_{0.2}O_2$-based SPEs and $Ce_{0.8}Sm_{0.2}O_2$-based SPEs, respectively.

These results were obtained without prior conditioning of the sensors. Potential for $t = 0$ was recorded immediately after immersing the dry electrodes in the sample solution. CeO_2-based SPEs do not require pre-treatment, which is a great advantage if we consider that the simple, plastic devices can be used as disposable sensors.

These results aimed to demonstrate the stability of CeO_2-based SPEs for continuous pH recording. Although the $Ce_{0.8}Sm_{0.2}O_2$-based SPEs were more sensitive than those obtained with a Sm stabilized ceria membrane [32], we cannot yet claim that $Ce_{0.8}Sm_{0.2}O_2$-based SPE oxides are better than CeO_2-based SPEs for pH measurements at 25 °C. Of all the CeO_2-based SPEs, $Ce_{0.8}Zr_{0.2}O_2$ SPEs have a wide linear pH range (from 5.3 to 13.2, at least). They also exhibit almost ideal Nernstian response (sensitivity $-(51 \pm 3)$mV/pH). $Ce_{0.8}Zr_{0.2}O_2$ SPEs appear, therefore, to be the electrodes best suited for accurate measurements. CeO_2-based SPEs were shown to reach the performance levels of those previously described in the literature [14] and to be more robust for semi-continuous measurements in alkaline media [36,37]. The reference electrode should be optimized for sustainability and robustness as was done with the sensors developed by Palchetti et al. [58] for field measurement of trace-elements.

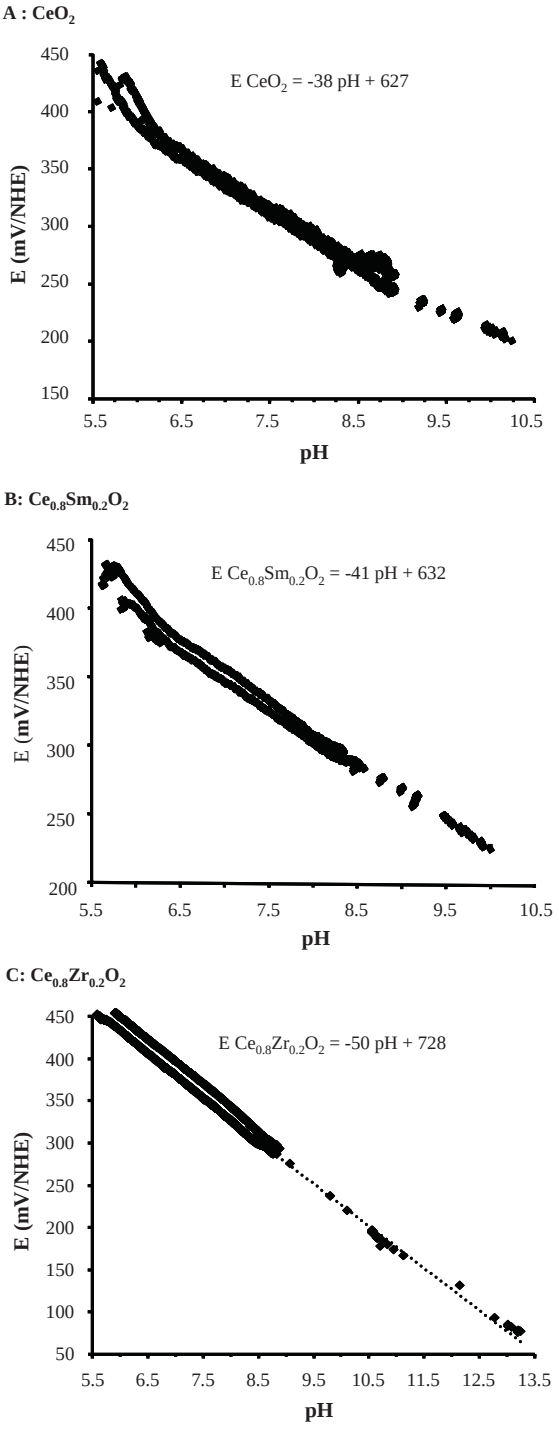

Fig. 9. Potential response of CeO_2-, $Ce_{0.8}Sm_{0.2}O_2$- and $Ce_{0.8}Zr_{0.2}O_2$-based SPEs obtained at 25 °C in continuous pH values in NaCl (0.1 mol L^{-1}) spiked with a $NaHCO_3/Na_2CO_3$ buffer (pH 10.5, ionic strength 0.2). The experiment was extended to pH 13.2 with NaOH (1 mol L^{-1}) for $Ce_{0.8}Zr_{0.2}O_2$-based SPEs.

4. Conclusions

This study investigated the possible use of CeO_2-based screen-printed electrodes (CeO_2 SPEs, $Ce_{0.8}Sm_{0.2}O_2$ SPEs and $Ce_{0.8}Zr_{0.2}O_2$ SPEs) for pH monitoring. The electrochemical behavior of CeO_2-based SPEs showed that they could be used as electrochemical sensors without the need for high input impedance equipment. The results of potentiometric analysis demonstrated the feasibility of using this technology to measure pH. CeO_2-based SPEs showed a near-Nernstian behavior in the pH range of 6–11 and the response was somewhat affected by the direction of the pH change. These seem to be well-suited to monitoring the pH (T = 25 °C) of the pore water in the COx formation during its evolution as a radioactive waste repository. CeO_2-based SPEs were successfully used for continuous monitoring of pH for 100 h.

Of the three types of electrodes studied, $Ce_{0.8}Zr_{0.2}O_2$ SPEs appear to be the most suitable for accurate measurements on site, probably because $Ce_{0.8}Zr_{0.2}O_2$ is the highest oxygen vacancy carrier. Vacuum-packed $Ce_{0.8}Zr_{0.2}O_2$ SPEs could be integrated in automatic probes containing carrousels on which several electrodes would be stored in order to do continuous monitoring of pH without any maintenance over long periods by automatically changing the working electrode. More strongly designed probes using the same components could be considered for pH measurements in radioactive waste repositories.

Acknowledgements

This work was funded by (i) a BRGM-ANDRA partnership (CAPTANDRA project 2009–2011, Dr. Stéphane Buschaert) and (ii) the Cyprus Research Promotion Foundation for funding project KYΓA/0907 NANOSENS (Cyprus-France Bilateral Collaboration). The authors would like to thank S. Gravani (University of Cyprus) for providing the powders.

References

[1] OECD Nuclear Energy Agency, Reversibility and retrievability in geologic disposal of radioactive waste: reflections at the international level, OECD, Paris, 2001.
[2] S. Glab, A. Hulanicki, G. Edwall, F. Ingman, Crit. Rev. Anal. Chem. 21 (1989) 29.
[3] A. Fog, R.P. Buck, Sens. Actuators B 5 (1984) 137.
[4] M.J. Tarlov, S. Semancik, K.G. Kreider, Sens. Actuators B 1 (1990) 293.
[5] J.V. Dobson, P.R. Snodin, H.R. Thirsk, Electrochim. Acta 21 (1976) 527.
[6] T. Katsube, I. Lauks, J.N. Zemel, Sens. Actuators B 2 (1982) 399.
[7] L.D. Burke, J.K. Mulcahy, D.P. Whelan, J. Electroanal. Chem. 163 (1984) 117.
[8] P.J. Kinler, J.E. Heider, Sens. Actuators B 22 (1994) 13.
[9] F. Yue, T.S. Ngin, G. Hailin, Sens. Actuators B 32 (1996) 33.
[10] J. Hendrikse, W. Olthuis, P. Bergveld, Sens. Actuators B 53 (1998) 97.
[11] M. Wang, S. Yao, M. Madou, Sens. Actuators B 81 (2002) 313.
[12] G.M. da Silva, S.G. Lemos, L.A. Pocrifka, P.D. Marreto, A.V. Rosario, E.C. Pereira, Anal. Chim. Acta 616 (2008) 36.
[13] K. Pasztor, A. Sekiguchi, N. Shimo, N. Kitamure, H. Masuhara, Sens. Actuators B 14 (1993) 561.
[14] R. Koncki, M. Mascini, Anal. Chim. Acta 351 (1997) 143.
[15] J.A. Mihell, J.K. Atkinson, Sens. Actuators B 48 (1998) 505.
[16] C. Colombo, T. Kappes, P.C. Hauser, Anal. Chim. Acta 412 (2000) 69.
[17] P. Shuk, K.V. Ramanujachary, M. Greenblatt, Electrochim. Acta 41 (1996) 2055.
[18] A. Eftekhari, Sens. Actuators B 88 (2003) 234.
[19] K. Arshak, E. Gill, A. Arshak, O. Korostynska, Sens. Actuators B 127 (2007) 42.
[20] H. Galster, pH Measurements—Fundamentals, Methods, Applications, Instrumentation, VCH, New York, 1991.
[21] C. Cachet-Vivier, B. Tribollet, V. Vivier, Talanta 82 (2010) 555.
[22] L.W. Niedrach, Science 207 (1980) 1200.
[23] L.W. Niedrach, J. Electrochem. Soc. 127 (1980) 2122.
[24] T. Tsuruta, D.D. Macdonald, J. Electrochem. Soc. 129 (1982) 1221.
[25] S. Hettiarachchi, D.D. Macdonald, J. Electrochem. Soc. 131 (1984) 2206.
[26] V.V. Kharton, F.M.B. Marques, A. Atkinson, Solid State Ionics 174 (2004) 135.
[27] Y. Inda, K. Yamashitaa, T. Umegaki, M. Greenblattb, Solid State Ionics 86–88 (1996) 1121.
[28] G.B. Balazs, R.S. Glass, Solid State Ionics 76 (1995) 155.
[29] K. Yamashita, K.V. Ramanujachary, M. Greenblatt, Solid State Ionics 81 (1995) 53.
[30] D.G. Brookins, Eh–pH Diagrams for Geochemistry, Springer-Verlag, New York, 1988.
[31] Y. Sugie, A. Mineshige, M. Kobune, S. Fujii, Thin Solid Films 250 (1994) 8.
[32] P. Shuk, K.V. Ramanujachary, M. Greenblatt, Solid State Ionics 85 (1996) 257.
[33] K. Polychronopoulou, J.L.G. Fierro, A.M. Efstathiou, J. Catal. 228 (2004) 417.
[34] S. Betelu, C. Vautrin-Ul, J. Ly, A. Chaussé, Talanta 80 (2009) 372.
[35] C. Parat, S. Betelu, L. Authier, M. Potin-Gautier, Anal. Chim. Acta 573–574 (2006) 14.
[36] H.N. McMurray, P. Douglas, D. Abbot, Sens. Actuators B 28 (1995) 9.
[37] L. Qingwen, L. Guoan, S. Youqin, Anal. Chim. Acta 409 (2000) 137.
[38] E.C. Gaucher, C. Tournassat, F.J. Pearson, P. Blanc, C. Crouzet, C. Lerouge, S. Altmann, Geochim. Cosmochim. Acta 73 (2009) 6470.
[39] K. Polychronopoulou, C.N. Costa, A.M. Efstathiou, Appl. Catal. A 272 (2004) 37.

[40] A. Cagnini, I. Palchetti, I. Lionti, M. Mascini, A.P.F. Turner, Sens. Actuators B 24 (1995) 85.
[41] J.E. Moneyron, A. de Roy, C. Forano, J.P. Besse, Appl. Clay Sci. 10 (1995) 163.
[42] O. Bagel, B. Limoges, B. Schollhorn, C. Degrand, Anal. Chem. 69 (1997) 4688.
[43] A.J. Bard, L. Faulkner, Electrochimie Principe, Méthodes et Applications, Masson, Paris, 1983.
[44] S. Betelu, C. Vautrin-Ul, A. Chaussé, Electrochem. Commun. 11 (2009) 383.
[45] D.D. Macdonald, S. Hettiarachchi, S.J. Lenhart, J. Solution Chem. 17 (1988) 719.
[46] L. Authier, B. Schöllhorn, B. Limoges, Electroanalysis 10 (1998) 1255.
[47] H. Iwahara, Solid State Ionics 77 (1995) 289.
[48] H. Iwahara, Solid State Ionics 86–88 (1996) 9.
[49] B.K. Narayanan, S.A. Akbar, P.K. Dutta, Sens. Actuators B 87 (2002) 480.
[50] R.C. Engstrom, V.A. Strasser, Anal. Chim. Acta 56 (1984) 136.
[51] J. Wang, P. Tuzhi, V. Villa, J. Electroanal. Chem. 234 (1987) 119.
[52] J. Wang, M. Pedrero, H. Sakslund, O. Hammerich, J. Pingarron, Analyst 121 (1996) 345.
[53] L. Bousse, H.H. van den Vlekkert, N.F. de Rooij, Sens. Actuators B 2 (1990) 103.
[54] Y.H. Liao, J.C. Chou, Sens. Actuators B 128 (2008) 603.
[55] C.R. Caflisch, L.R. Pucacco, N.W. Carter, Kidney Int. 14 (1978) 126.
[56] J.P. Hoare, The Electrochemistry of Oxygen, Interscience Publication, New York, 1968, p. 19.
[57] J. Schüring, H.D. Schulz, W.R. Fischer, Redox: Fundamentals, Processes and Applications, Springer-Verlag, Berlin, Heidelberg, New York, London, Paris, Tokyo, Hong Kong, Barcelona, Budapest, 1999.
[58] I. Palchetti, S. Laschi, M. Mascini, Anal. Chim. Acta 530 (2005) 61.